Designing a ternary photovoltaic cell for indoor light harvesting with a power conversion efficiency exceeding 20%

Yin, Hang; Ho, Johnny Ka Wai; Cheung, Sin Hang; Yan, Roger Jie; Chiu, Ka Lok; Hao, Xiaotao; So, Shu Kong

Published in:
Journal of Materials Chemistry A

DOI:
10.1039/c8ta01728j

Published: 14/05/2018

Document Version:
Peer reviewed version

Designing a Ternary Photovoltaic Cell for Indoor Light Harvesting with a Power Conversion Efficiency Exceeding 20%

Hang Yin,[a] Johnny Ka Wai Ho,[a] Sin Hang Cheung,[a] Roger Jie Yan,[a] Ka Lok Chiu,[a] Xiaotao Hao[b] and Shu Kong So[a,*]

[a.] *Department of Physics and Institute of Advanced Materials, Hong Kong Baptist University, Kowloon Tong, Hong Kong SAR, P. R. China.*

[b.] *School of Physics, State Key Laboratory of Crystal Materials, Shandong University, Jinan, Shandong, P. R. China*

We use several polymers as the ternary component to demonstrate a ternary strategy to improve the performance of PCDTBT:$PC_{71}BM$ devices under 1-Sun and indoor illuminances. With a binary bulk-heterojunction (BHJ) of PCDTBT:$PC_{71}BM$ organic photovoltaic (OPV) cell, a power conversion efficiency (PCE) of 16.5% under indoor light sources (300 lux from fluorescence tube). However, with a ternary BHJ cell of PCDTBT:PDTSTPD:$PC_{71}BM$, the PCE can be enhanced to 20.8%. FFs are the main improvements. Transport and absorption measurements indicate the origins of the improvements of OPV performance: the ternary BHJ films exhibit enhanced hole mobilities, and reduced Urbach energies, indicating that the blending of the PDTSTPD component passivates shallow traps near the band edge of the BHJ films.

Introduction

The advent of the Internet of Things (IoT) transforms the ways we work and live. It is estimated that more than 50 billion Internet- enabled objects, such as cellphones, wearable devices and sensors will be connected into the IoT network by the year of 2020.[1] Such huge amounts of separate and off-grid gadgets presumably require light-weight portable batteries, and how these batteries can be charged in time and conveniently presents a big challenge. Currently, several candidates, with power in the range of 1-100 μW, are under consideration and they mainly involve piezoelectricity and vibrational energy.[2-4] As IoTs are usually operated indoor, few people pay attention to photovoltaic (PV) devices because they are developed for outdoor application.[5-10] So IoTs and PV cells should not overlap.

The rise of organic photovoltaic (OPV) cells, however, is altering the relationship between IoTs and PV cells. Organic materials possess strong absorbances in the visible light region ~390-760nm,[11-14] and so OPV cells are better light harvestors than silicon-based PV devices under room light illumination. This realization spearheads the emergent study of OPV devices under different illumination conditions.[15-18] As reported by Cutting *et al.*, the power conversion efficiencies (PCEs) (under 1-Sun) of P3HT:PCBM and PTB7-Th:$PC_{71}BM$ bulk-heterojunction (BHJ) cells were around 2.93% and 8.65%, and surged up to around 12.83% and 20.19%, respectively, under the LED illuminations.[19] As a comparison, the c-Si-based PV device achieves a PCE of 16.72% under the 1-Sun illumination, and only increases moderately to 20.19% under white

LED illumination. PCDTBT, a well- known donor polymer used in OPV, has been the focus of attention lately because its OPV cells possess relatively high V_{oc} (~0.9V).[20,21] It has been observed PV devices generally suffer from a loss of V_{oc} of about 0.2V under room lighting conditions. Therefore PV devices with a higher V_{oc} like PCDTBT will be able to retain a large fraction of its V_{oc} under room illuminations. Using this concept, Lee *et al.* compared the performances of PTB7:$PC_{71}BM$, and PCDTBT:$PC_{71}BM$ OPV devices under various illuminations.[22] Under 1-Sun, their PTB7:$PC_{71}BM$ device achieved a higher PCE of 6.8%. But under 300 lux of fluorescent light (FL) illumination, the PCDTBT:$PC_{71}BM$ cell achieved a higher PCE of 16.6%. This observation clearly shows the potential of PCDTBT-based OPV devices under indoor illumination.

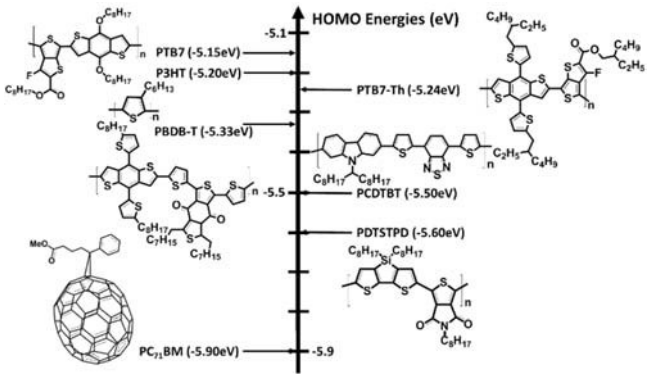

Figure 1. Chemical structures and HOMO levels of PCDTBT, $PC_{71}BM$; polymers used as the ternary elements are PTB7, PTB7-Th, PBDB-T, P3HT, and PDTSTPD.

One problem related to the BHJ of PCDTBT:$PC_{71}BM$ is its relatively poor hole transport, which impacts negatively on the device fill-factor (FF) and short-circuit current (J_{sc}). To overcome this problem, a ternary BHJ cell can be considered. Specific functionalities of ternary components can improve the performance of OPV cells: (i)

enhanced carrier mobilities improve FFs23,24; (ii) complementary optical absorptions increase J_{sc}s[25,26]; and (iii) matched energy levels enlarge V_{oc}s[27,28]. In this study, we adopt a ternary strategy and improve the performance of PCDTBT-based OPV devices. PCDTBT is chosen as the host polymer because it has a large V_{oc} of 0.9V under 1 Sun. Despite this advantage, PCDTBT:$PC_{71}BM$ has inferior hole mobilities in the range of ~$10^{-5}cm^2V^{-1}s^{-1}$. Thus if a ternary polymer with a high hole mobility is introduced, it is anticipated that the PCE of the resulting ternary cells would be improved. Following this idea, five well-studied polymers, namely, PTB7, PTB7-Th, P3HT, PBDB-T, and PDTSTPD are chosen as the ternary candidates. The BHJ cells have a general composition of donor-1 (host):donor-2 (ternary polymer):$PC_{71}BM$ weight ratio of 0.9:0.1:2. The overall donor:acceptor weight ratio is fixed at 1:2. Among all cells, the PCDTBT:PDTSTPD:$PC_{71}BM$ cell achieves the highest PCE of 19.8% under 300 lux of illuminance from the 2700K FL tube. By the solvent vapor annealing (SVA), the PCE can be further enhanced to 20.8%. To investigate the origins of the improved OPV performances, we use admittance spectroscopy (AS) to measure the field dependent hole mobilities of the optimized ternary and binary BHJ films. We found that the ternary BHJ has improved hole transports. In addition, photothermal deflection spectroscopy (PDS) was performed to measure the subgap optical absorptions of the BHJ films. It was found that the ternary BHJ has sharpened band edge, implying the passivation of shallow traps near the band edge in ternary BHJs.

Experimental

The OPV device structure was ITO/PEDOT:PSS/BHJ/LiF/Al. The indium tin oxide- (ITO-) patterned glass substrates were ultrasonicated subsequently in deionized water, acetone, and 1,2- propanol, and then dried in ambient air overnight. After a 13 mins UV-ozone treatment, a PEDOT:PSS layer was spin-coated on the cleaned substrate at 7000 rpm for 60s, which was further annealed on a 140^{o}C hotplate for 10 mins. The resulting PEDOT:PSS layer had a thickness of 30nm. The substrates were then transferred into a N2 filled glove box to spin-coat the active layers. Polymers for BHJ cells fabrication were obtained from 1-Materials, and $PC_{71}BM$ was obtained from Nano-C. They were mixed in the appropriate ratios. For the binary BHJ, the donor:acceptor (D:A) weight ratio was fixed as 1:2, and for ternary systems, the PCDTBT:polymer:$PC_{71}BM$ weight ratio was 0.9:0.1:2. The overall donor concentration was 7mg/mL in clorobeneze (CB), and the spin speed was 1600rpm for 60s, to form ~85nm uniform active layers. The ternary polymers were PTB7, PTB7- Th, P3HT, PBDB-T, and PDTSTPD. Finally, a thin LiF layer (~1nm) and Al cathode (~130nm) were evaporated in a high vacuum chamber (~$4x10^{-6}$ torr).

Performance under 1-Sun

Figure 1 summarizes the chemical structures and HOMO/LUMO levels of the host polymer PCDTBT, the acceptor $PC_{71}BM$, and the ternary polymers. PCDTBT and PDTSTPD have relatively low lying HOMO levels (-5.50eV and -5.60eV, respectively), which are more favorable to fabricate large-V_{oc} OPV devices. Figure 2 displays the

current density-voltage (J-V) characteristics of the binary PCDTBT:$PC_{71}BM$, and ternary PCDTBT:polymer:$PC_{71}BM$ devices under 100 mW/cm□ of AM 1.5G solar illumination. The binary control device achieves an overall PCE of 5.3%, with a J_{sc} of 10.8mA/cm2, FF of 56.0%, and V_{oc} of 0.87V. The PCDTBT:PTB7-Th:$PC_{71}BM$ and PCDTBT:PTB7:$PC_{71}BM$ ternary cells exhibit enhanced J_{sc} in excess of 11.2mA/cm2. However, V_{oc} of these two ternary devices drop to 0.85V and 0.82V, respectively. Among these polymers, PDTSTPD is a promising ternary candidate because it has a similar chemical structure to PCDTBT, a relatively higher hole mobility and a low lying HOMO level, and stronger optical absorptions in the near infrared region.[29,30] The PCDTBT:PDTSTPD:$PC_{71}BM$ cell achieves an optimized overall PCE of 6.0%, J_{sc} of 11.2mA/cm^2, FF of 60.2%, and V_{oc} of 0.89V. The PCE of the ternary cell with PDTSTPD can be further enhanced to 6.3% (J_{sc} of 11.0mA/cm^2, FF of 63.1%, and V_{oc} of 0.90V) by solvent vapor annealing (SVA) using tetrahydrofuran (THF) for 30s. (**Figure S1**) The origin of PCE enhancement from SVA is not clear. But it is likely to originate from the improvement of morphology from similar works.[31,32] **Table 1** summarizes the OPV parameters of the binary and ternary OPV devices with various ternary compounds.

Performance under Indoor Illumination

We further examined PCDTBT:PDTSTPD:$PC_{71}BM$ ternary devices under indoor light conditions. Commercially available T5 tubes were used to simulate the indoor lights: LED (model PAK410080) with color temperatures of 3000 K, 4000 K, and 6500

K; and FL (model PAK300408) with color temperature of 2700 K, 4000 K, and 6500 K. The emission spectra $S(\lambda)$ of the tubes were acquired, and **Figure 3(a)** depicts the LED emission spectra normalized by its total emission intensity ($\int_{\text{visible}} S(\lambda)\mathrm{d}\lambda$ in Eq. (2)), so that the area under each curve in the figure is 1. The spectra for all light sources are shown in the supplementary information **Figure S2**. FL spectra originate from fluorescence of phosphors and emission from excited Hg vapor inside the lamp, producing characteristic peaks of narrow bands, while LED spectra are produced from emission of a combination of a GaN blue LED and fluorescence of phosphor materials, giving a broad spectrum with a peak in the blue color region.[33,34] Stronger optical emission is observed in the near ultraviolet region (450-460 nm) for high color temperature tubes, but in the near infrared region for lower color temperature tubes. An illuminance of 300 lux is a widely recognized indoor standard used in the lighting industry.[19,21] Therefore, the distance between devices and light tubes were adjusted in our experiments such that the total illuminance was fixed at 300 lux (measuring with the Lutron LX-102 photometer). The input power intensities of various light sources were then calculated based on the illuminance. For a monochromatic light source, the relationship between the illuminance L and the power intensity I can be expressed as[14]

$$L(\lambda) = K_{\mathrm{r}} I V(\lambda) \qquad (1)$$

where K_{r} is a constant scaling factor of 683 $\mathrm{lm/W}$ (the maximum spectral luminous

efficacy for human photopic vision), and $V(\lambda)$ [**Figure 3(b)**] is the CIE 1988 2° spectral luminous efficiency function for human photopic vision deduced to be adopted by the photometer.[35] Due to the spectral sensitivity of human eyes, the effective brightness, namely illuminance, needs to be weighed by $V(\lambda)$ which accounts for the visual sensitivity. For heterochromatic light sources, the total illuminance L involves the integral of the emission spectrum of photopic vision, $S(\lambda)$ x $V(\lambda)$, over the visible region, i.e.

$$L = K_{\mathrm{r}} I \frac{\int_{visible} S(\lambda)V(\lambda)d\lambda}{\int_{visible} S(\lambda)d\lambda} \qquad (2)$$

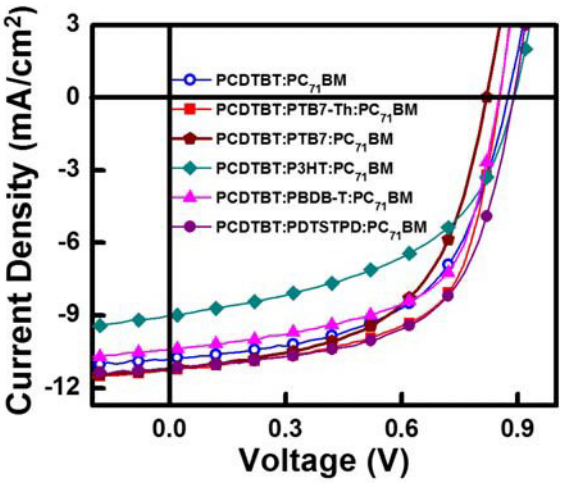

Figure 2. JV characteristics of the binary PCDTBT:$PC_{71}BM$ and ternary OPV devices with different ternary compounds under 100mW/cm^2 of AM 1.5G solar illumination. The PCDTBT: Ternary Compound: Fullerene weight ratio is fixed as 0.9:0.1:2.

Ternary Polymers	V_{oc} (V)	J_{sc} (mA/cm^2)	FF (%)	PCE (%)
Nil	0.87	10.8	56.0	5.3
P3HT	0.89	9.0	49.9	4.0
PTB7-Th	0.85	11.3	61.6	5.9
PBDB-T	0.85	10.4	60.0	5.3
PDTSTPD	0.89	11.2	60.2	6.0
PTB7	0.82	11.2	55.8	5.1

Table 1. OPV parameters of the binary PCDTBT:$PC_{71}BM$ and ternary PCDTBT:ternary polymer:$PC_{71}BM$ OPV devices under 1-Sun illumination. The binary BHJ has a donor:acceptor composition of 1:2. The ternary BHJs have a composition of donor1:donor2:acceptor composition of 0.9:0.1:2, where donor 2 is the ternary polymer.

Figure 3(c) shows the distribution of normalized $S(\lambda)$ x $V(\lambda)$, which is essentially the product of **Figure 3(a)** and **3(b)**. The input power intensity can be calculated by Eq. (2). The last column of **Table 2** shows the calculated input powers (P_{in}) arising from different light sources. Different emission spectra possess different overlapping with $V(\lambda)$ and hence the integral value, so under the fixed 300 lux illumination, the input power intensity is the smallest for the spectrum with the best overlapping. Nonetheless, the computed P_{in}'s are similar for all light sources used here ranged 74-80 μW/cm^2. The results are also comparable to those reported elsewhere under the same illuminance of 300 lux.[17,22]

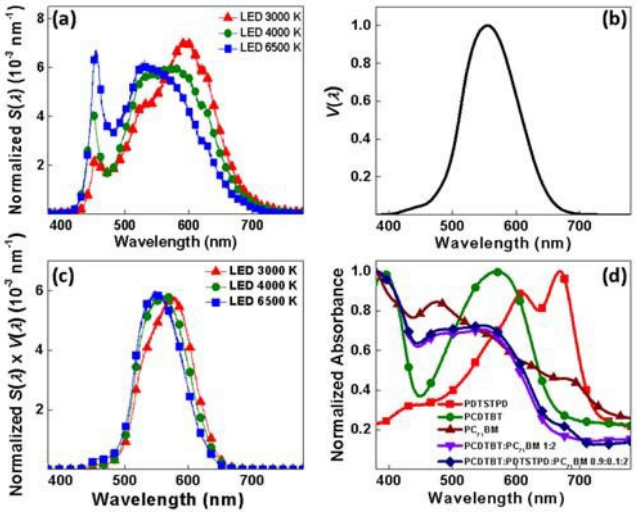

Figure 3. (a) Normalized emission spectra of the LED light sources normalized by total intensity with color temperatures 3000 K, 4000 K, and 6500 K; (b) human photopic spectra luminous efficiency function[14]; (c) distribution of normalized $S(\lambda)$ x $V(\lambda)$; and (d) normalized UV-visible absorption spectra of the binary and ternary BHJ films, and individual materials. The thicknesses of films are about 85nm, which is the thickness of the optimized BHJ devices.

Figure 4 shows the JV characteristics of the binary PCDTBT:$PC_{71}BM$ and ternary PCDTBT:PDTSTPD:$PC_{71}BM$ OPV devices under different indoor illuminations with a fixed illuminance of 300 lux: (a,b) FL sources; (c,d) LED sources. The ternary cells consistently exhibit enhanced OPV parameters in all cases. Under a 2700K FL tube, a highest PCE of 19.8% is achieved for the ternary cell. The OPV performance of binary PCDTBT:$PC_{71}BM$ cells is similar to those recently reported by Lee *et. al.*[22] For the ternary cells, the J_{sc} improvement is mainly contributed by the enhanced optical absorption in the near the infrared region. **Figure 3(d)** displays the normalized UV-

visible absorption spectra of the binary and ternary BHJ films, and their pure compound layers. There is a small, but distinct absorption peak between 650-700 nm for the ternary film, which matches the absorption peak of PDTSTPD. The performance of ternary cells can be further improved by SVA for 30s after the spin coating of BHJ films. Under a 2700K FL tube, the ternary cell with SVA achieves an optimized PCE of 20.8%, with the V_{oc} of 0.73V, FF of 63.5%, and J_{sc} of 33.3 μ A/cm^2. However, when OPV devices are illuminated by other indoor light sources with higher color temperatures, the J_{sc} differences between binary and ternary cells become smaller because of the mismatches of the emission and absorption spectra. For example, when devices are illuminated under a 6500K LED tube, both the binary and ternary cells show reduced J_{sc} and overall PCEs. J_{sc} of the ternary and binary cells decreases significantly to 29.0μA/cm^2 and 28.3μA/cm^2, resulting in PCEs of 16.1% and 13.9%, respectively. The OPV parameters of the binary PCDTBT:$PC_{71}BM$ and ternary PCDTBT:PDTSTPD:$PC_{71}BM$ BHJ solar cells are summarized in Table 2. Improvements in FF and V_{oc} in ternary cells can be observed under various light sources. However, PCDTBT-based solar cells achieve higher J_{sc} under neutral (4000K) and warm (2700K & 3000K) light sources, than cool (6500K) FL and LED tubes. **Figure 5** summarizes the PCEs and output powers of binary PCDTBT:$PC_{71}BM$, ternary PCDTBT:PDTSTPD:$PC_{71}BM$ cells with or without SVA under different indoor light sources.

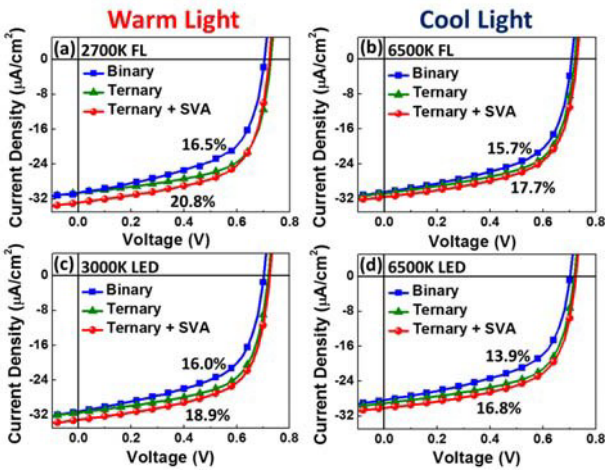

Figure 4. JV characteristics of binary PCDTBT:$PC_{71}BM$ and ternary PCDTBT: PDTSTPD:$PC_{71}BM$ OPV devices under different indoor illuminations with a fixed illuminance of 300 lux: (a,b) FL sources; (c,d) LED sources.

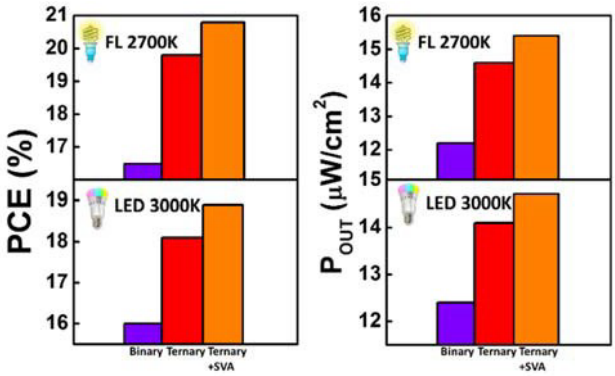

Figure 5. PCEs and output powers of binary PCDTBT:PC71BM, ternary PCDTBT:PDTSTPD:PC71BM cells with or without SVA under different indoor light sources.

Color Temperature (K)	Light Source	BHJ	SVA	FF (%)	V_{oc} (V)	J_{sc} (μA/cm^2)	PCE (%)	P_{out} (μW/cm^2)	P_{in} (μW/cm^2)
2700	FL	Binary		56.4	0.70	30.7	16.5	12.2	74.0
		Ternary		61.7	0.72	32.8	19.8	14.6	
		Ternary	√	63.5	0.73	33.3	20.8	15.4	
3000	LED	Binary		56.6	0.70	31.2	16.0	12.4	77.6
		Ternary		62.1	0.72	31.4	18.1	14.1	
		Ternary	√	61.1	0.73	33.1	18.9	14.7	
4000	FL	Binary		56.1	0.70	29.9	14.6	11.8	80.8
		Ternary		61.9	0.72	30.6	16.8	13.6	
		Ternary	√	61.4	0.73	33.1	18.3	14.8	
4000	LED	Binary		56.6	0.70	31.2	16.2	12.5	77.0
		Ternary		62.5	0.72	31.6	18.4	14.2	
		Ternary	√	61.0	0.73	32.8	19.0	14.6	
6500	FL	Binary		57.7	0.71	30.5	15.7	12.4	79.2
		Ternary		61.2	0.72	30.8	17.1	13.5	
		Ternary	√	60.9	0.73	31.6	17.7	14.0	
6500	LED	Binary		55.4	0.70	28.3	13.9	11.0	79.4
		Ternary		61.3	0.70	29.0	16.1	12.8	
		Ternary	√	61.0	0.72	30.1	16.8	13.3	

Table 2. OPV parameters of binary PCDTBT:$PC_{71}BM$ and ternary PCDTBT:PDTSTPD:$PC_{71}BM$ solar cells under various indoor light sources.

Discussions:

(A) How to choose PV materials for room lights

Below, we briefly discuss why a large V_{oc} is essential for making BHJ cells for room light harvesting. The V_{oc} loss under room lights can be rationalized by dependence of V_{oc} on the light dependent photocurrent I_{ph}:

$$V_{\mathrm{oc}} \approx \frac{nkT}{q} \ln \frac{I_{\mathrm{ph}}}{I_{\mathrm{o}}} \qquad (3)$$

where n is the ideality factor of the diode, k is the Boltzmann constant, T is the cell temperature, q is the electron charge, and I_0 is the dark current.[22] Two observations can be deduced from Eq. (3). First, under a fixed illumination, material with a small dark current should give rise to a large V_{oc}. Thus, an OPV polymer with a large energy gap should give a large V_{oc}. Second, the reduction of V_{oc} (ΔV) under room lights can be expressed as

$$\Delta V = \frac{nkT}{q} \ln \frac{I_{ph,sun}}{I_{ph,room}} \qquad (4)$$

where $I_{\text{ph,sun}}$ and $I_{\text{ph,room}}$ are the photocurrents under 1-Sun and room lights, respectively. Note that ΔV is clearly independent of I_0. Furthermore, for most OPV materials, I_{ph} scales as the incident photon flux. In particular, $I_{\text{ph}} \sim P'^{\alpha}$ where P' is the incident power intensity contributed by the range of wavelength giving rise to photovoltaic effect, and α is a constant ranging from 0.75 in the case of space-charge limited photocurrent to unity for the space-charge-free limit.[36] Here we take the space-charge free limit ($\alpha \approx 1$) due to absence of charge injection. The solar spectrum consists of a wide range of infrared light which contributes little to the PV performance, while LED and FL spectra mostly cover only the visible region which corresponds to PV performance. We therefore write $P'_{\text{sun}} = P_{\text{sun}}\theta$ where $P_{\text{sun}} \approx 100$ mW/cm^2 is the nominal incident power intensity of 1-sun illumination and θ is its fraction of light without infrared (< 780 nm, defined by the range of $V(\lambda)$ corresponding to photopic vision). Then Eq. (4) can be written as

$$\Delta V \approx \frac{\propto nkT}{q} \ln \frac{P_{\text{sun}}\theta}{P_{\text{room}}} \quad (5)$$

and the V_{oc} of room light illumination can be expressed as

$$V_{\text{oc,room}} \approx V_{\text{oc,sun}} - \frac{\propto nkT}{q} \ln \frac{P_{\text{sun}}\theta}{P_{\text{room}}} \quad (6)$$

By investigating the area under the solar spectrum, 56.65% of the solar power comes from wavelength less than 780 nm. Using $P_{\text{room}} \approx 80\ \mu\text{W/cm}^2$ (~300 lux) in our experiment and assuming $n \approx 1$, we get a computed V_{oc} loss ΔV ≈0.166 V, which is almost the same loss as the experimental value (Table 2). It can be seen from Eq. (5) that ΔV should be independent of the choice of materials. We therefore conclude that to achieve a large V_{oc} at ambient lights, a BHJ that gives a large V_{oc} under 1-Sun is essential.

Recently, two papers report high-V_{oc} OPV devices used in room illuminations. *Lee* et al. fabricated BTR:$PC_{71}BM$ BHJ cells (V_{oc} of 0.945V under standard 1-Sun) and achieved an overall PCE of 28.1% under 1000 lux fluorescent lamps. Notably, under the indoor light, V_{oc} of the BTR:$PC_{71}BM$ device is 0.791V, which is the highest value among OPV cells used as indoor light harvesters.[37] *Yang* et al. used P3HT as the donor, and compared performance of P3HT-based devices with different acceptors in various illuminations.[38] Under 1- Sun, the P3HT:ICBA and P3HT:PCBM cells have a V_{oc}s of 0.89V and 0.59V, respectively. Therefore, under indoor illuminations (500 lux from

FL and LED), the P3HT:ICBA device achieves a leading V_{oc} of 0.73V, whereas V_{oc} of the P3HT:PCBM cell decreases to only 0.43V.

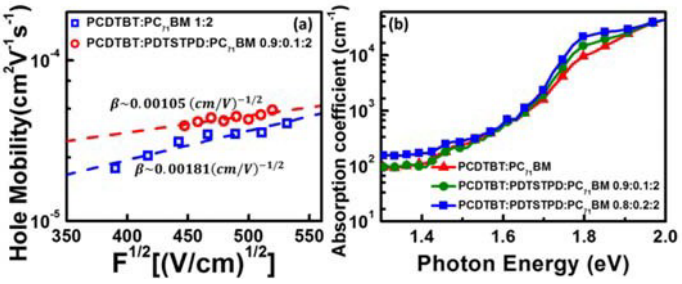

Figure 6. (a) Hole mobilities of binary PCDTBT:$PC_{71}BM$ and ternary PCDTBT:PDTSTPD:$PC_{71}BM$ BHJ films as a function of electric field; (b) subgap optical absorption spectra extracted from PDS for binary and ternary BHJ films with different weight fractions of PDTSTPD.

(B) How does the ternary PDTSTPD enhances PCEs under room lights

With a large V_{oc}, the next step is to improve the FF. Our ternary approach addresses how the ternary polymer enhances the FF by improving the electronic properties of the BHJs.

***Electronic Characterization*:** Admittance spectroscopy (AS) was performed to investigated the origins of the FF enhancements in ternary devices. The principle of AS is documented elsewhere.[39-41] The hole mobilities of the binary PCDTBT:$PC_{71}BM$ and ternary PCDTBT:PDTSTPD:$PC_{71}BM$ BHJ films were examined by AS. The hole-only device structure is ITO/PEDOT:PSS/BHJ/CuPc:Spiro-TPD/Au. **Figure 6(a)** shows the electric field dependent hole mobilities of binary and ternary BHJ films from AS

measurements at room temperature. The hole mobilities can be described by the Poole- Frenkel model which is expressed as

$$\mu(F) = \mu_0 \exp\left(\beta F^{1/2}\right) \qquad (7)$$

where μ_0 is the zero-field hole mobility, β is the Poole-Frenkel slope, and F is the applied electric field.[42] μ_0 and β are extracted to compare the hole transport properties. For the ternary BHJ film, $\mu_0 \approx 1.4 \times 10^{-5}$ $cm^2V^{-1}s^{-1}$, which is about half order larger than 4.4×10^{-6} $cm^2V^{-1}s^{-1}$ of the binary film. Meanwhile, the ternary film achieves a smaller Poole-Frenkel slope β of 1.05×10^{-3} $(cm \cdot V)^{1/2}$ than 1.81×10^{-3} $(cm \cdot V)^{1/2}$ of the binary film. A smaller β improves hole mobilities in the low field region, and enhances the charge balance near the V_{oc} condition.[43] Therefore, the PCDTBT:PDTSTPD:$PC_{71}BM$ ternary OPV devices achieve enhanced FFs than their counterpart binary control cells under 1-Sun and indoor light illuminations.

Photothermal deflection spectroscopy (PDS) was performed to investigate the subgap bandedge absorption of the BHJ films. A sharper bandedge, associated with a more abrupt drop in the absorption just below the bandgap energy, is an indication of reduced disorder.[44] For organic amorphous semiconductors, the optical absorption coefficient α mean the bandedge can be expressed as

$$\alpha = \alpha_0 \exp\left[\frac{h\nu - E_g}{E_u}\right] \qquad (8)$$

where $\boldsymbol{\alpha_0}$ is the optical absorption coefficient at the bandgap, $\boldsymbol{h\nu}$ is the photon

energy, and E_u is the Urbach energy. E_u can be used to describe the width of the localized band tail states.[45] A small E_u indicates a faster drop in the optical absorption just below the bandgap energy E_g, a narrower band tail, and reduced shallow traps. **Figure 6(b)** shows the subgap optical absorption spectra of PCDTBT- based binary and ternary BHJ films from PDS measurements. The reduction of E_u can be clearly observed in the ternary films. E_u is 53.4 meV for the PCDTBT:$PC_{71}BM$ binary film, and decreases to 43.1 meV in the ternary film with 10% ternary PDTSTPD in weight. Correspondingly, the optimized ternary solar cell (10% PDTSTPD) achieves an enhanced FF of 60.2% than 56.0% of the binary control device. However, although E_u is further decreased to 39.6meV in the ternary film with 20% PDTSTPD in weight, the FF and PCE decrease to 55.7% and 5.6%, respectively, because of the excessive subgap traps shown in Figure 6(b). AS and PDS results indicate that PDTSTPD molecules behave as conducting linkers for PCDTBT molecules. Shallow defects near the bandedge are passivated, and energetic disorders of hole transport are reduced in the ternary BHJ films, resulting in suppressed PF effects of hole transport and improved hole mobilities.

Conclusions

We propose a ternary strategy to improve the OPV performance of PCDTBT:PC71BM devices under 1-Sun and indoor illuminances. A low HOMO (-5.6 eV) polymer PDTSTPD is selected as the ternary compound with the D1:D2:A weight ratio

is 0.9:0.1:2. Under the 1- Sun illumination, the ternary device achieves an enhanced PCE of 6.0%, than 5.3% of the binary device. The ternary cells also exhibit improved OPV performances under different indoor light sources (300 lux). A high PCE of 20.8% was achieved under 300 lux of illumination from a 2700K FL tube. FFs are the main improvements. Meanwhile, ternary cells tend to have higher J_{sc} under indoor tubes with lower color temperatures due to better spectral overlap of the emission spectra of light sources, and the absorption spectra of ternary BHJ films. Transport and absorption measurements are performed to reveal the origins of the improvements of OPV performances in ternary devices. With the ternary polymer PDTSTPD, the BHJ films exhibit enhanced hole mobilities and smaller Poole-Frenkel slopes β. Meanwhile, the sharpening of the bandgap (reduced E_{u}) be clearly observed in the ternary films, indicating that the blending of PDTSTPD passivates the shallow traps near the bandedge of the PCDTBT:$PC_{71}BM$ BHJ films. The present study suggests that some polymers that have been abandoned because of large bandgaps and "poor" hole transporting capability should be re- considered under different illuminations. PCDTBT fits into this category. This polymer shows much better spectral overlap with room lights and its transport can be much enhanced using a ternary polymer. Its BHJ solar cells clearly outperform the conventional "high" performance polymer. We believe PCDTBT is not the lone outlier and more polymers with similar potentials can be identified in future.

Conflicts of interest

There are no conflicts to declare

Acknowledgements

Support of this research by the RGC of Hong Kong and NSFC of China under Grant # N_HKBU202/16 is gratefully acknowledged. X. T. H. acknowledges the National Natural Science Foundation of China for the NSFC/RGC project (No. 61631166001.)

Notes and references

1 Nordrum, Popular Internet of Thins Forecast of 50 Billion Devices by 2020 is Outdated, *IEEE*, 2016.

2 Y. Hu, H. Xue, H. Hu, *Smart Mater. Struct*. 2007, **16**.

3 T. M. Kamel, R. Elfrink, M. Renaud, D. Hohlfeld, M. Goedbloed, C. d. Nooijer, M. Jambunathan, R. v. Schaijk, *J. Micromech. Microeng*. 2010, **20**, 105023.

4 S. P. Beeby, M. J. Tudor, N. M. White, *Meas. Sci. Technol*. 2006, **17**, R175.

5 M. A. Green, K. Emery, Y. Hishikawa, W. Warta, E. D. Dunlop, *Prog. Photovoltaics*. 2015, **23**, 1.

6 Q. Fan, W. Su, X. Meng, X. Guo, G. Li, W. Ma, M. Zhang, Y. Li, *Sol. RRL*, 2017, **1**, 1700020.

7 M. Jørgensen, K. Norrman, F. C. Krebs, Stability/Degradation of Polymer Solar

Cells. *Sol. Energ. Mat. Sol. C*. 2008, **92**, 686.

8 Z. He, C. Zhong, S. Su, M. Xu, H. Wu, Y. Cao, *Nat. Photonics*. 2012, **6**, 591.

9 J. Yan, Q. Liang, K. Liu, J. Miao, H. Chen, S. Liu, Z. He, H. Wu, J. Wang, Y. Cao, *ACS Energy Lett*. 2017, **2**, 14.

10 D. Yang, H. Sasabe, T. Sano, J. Kido, *ACS Energy Lett*. 2017, **2**, 2021.

11 M. Freitag, J. Teuscher, Y. Saygili, X. Zhang, F. Giordano, P. Liska, J. Hua, S. M. Zakeeruddin, J. Moser, M. Grätzel, A. Hagfeldt, 2017, **11**, 372.

12 H. Hoppe, N. S. Sariciftci, *J. Mater. Res*. **2004**, *19*, 1924-1945.

13 D. Xie, T. Liu, W. Gao, C. Zhong, L. Huo, Z. Luo, K. Wu, W. Xiong, F. Liu, Y. Sun, C. Yang, *Sol. RRL*. 2017, **1**, 1700044.

14 F. Archet, D. Yao, S. Chambon, M. Abbas, A. D'Aléo, G. Canard, M. Ponce-Vargas, E. Zaborova, B. L. Guennic, G. Wantz, F. Fages, *ACS Energy Lett*. 2017, **2**, 1303.

15 Y. Aoki, *Org. Electron*. 2017, **48**, 194.

16 F. D. Rossi, T. Pontecorvo, T. M. Brown, *Appl. Energ*. 2015, **156**, 413.

17 B. P. Lechêne, M. Cowell, A. Pierre, J. W. Evans, P. K. Wright, A. C. Arias, *Nano Energy* **2016**, *26*, 631.

18 M. Freitag, J. Teuscher, Y. Saygili, X. Zhang, F. Giordano, P. Liska, J. Hua, S. M. Zakeeruddin, J. Moser, M. Grätzel, A. Hagfeldt, *Nat. Photonocs*, 2017, **11**, 372.

19 C. L. Cutting, M. Bag, D. Venkataraman, *J. Mater. Chem. C*. 2016, **4**, 10367.

20 J. S. Moon, J. Jo, A. J. Heeger, *Adv. Energy Mater*. 2012, **5**, 304.

21 M. A. Cowell, B. P. Lechene, P. Raffone, J. W. Evans, A. C. Arias, P. K. Wright, *J. Phys. Conf. Ser*. 2016, **773**, 012033.

22 H. K. H. Lee, Z. Li, J. R. Durrant, W. C. Tsoi, *Appl. Phys. Lett*. 2016, **108**, 253301.

23 G. Zhang, K. Zhang, Q. Yin, X. Jiang, Z. Wang, J. Xin, H. Yan, F. Huang, Y. Cao, *J. Am. Chem. Soc*. **2017**, *139*, 2387.

24 J. Zhang, Y. Zhang, J. Fang, K. Lu, Z. Wang, W. Ma, Z. Wei, *J. Am. Chem. Soc*. **2015**, *137*, 8176.

25 L. Nian, K. Gao, F. Liu, Y. Kan, X. Jiang, L. Liu, Z. Xie, X. Peng, T. P. Russell, Y. Ma, *Adv. Mater*. **2016**, *28*, 8184.

26 T. Liu, L. Huo, X. Sun, B. Fan, Y. Cai, T. Kim, J. Y. Kim, H. Choi, Y. Sun, *Adv. Energy Mater*. **2016**, *6*, 1502109.

27 R. A. Street, D. Davies, P. P. Khlyabich, B. Burkhart, B. C. Thompson, *J. Am. Chem. Soc*. **2013**, *135*, 986.

28 P. P. Khlyabich, B. Burkhart, B. C. Thompson, *J. Am. Chem. Soc*. **2012**, *134*, 9074.

29 H. Yin, K. L. Chiu, C. H. Y. Ho, H. K. H. Lee, H. W. Li, Y. Cheng, S. W. Tsang, S. K. So, *Org. Electron*. 2017, **40**, 1.

30 S. Chen, C. E. Small, C. M. Amb, J. Subbiah, T. Lai, S. Tsang, J. R. Manders, J. R. Reynolds, F. So, *Adv. Energy Mater*. 2012, **2**, 1333.

31 S. Miller, G. Fanchini, Y. Lin, C. Li, C. Chen, W. Su, M. Chhowalla, *J. Mater. Chem*. **2008**, *18*, 306.

32 Y. Zhao, Z. Xie, Y. Qu, Y. Geng, L. Wang, *Appl. Phys. Lett*. **2007**, *90*, 043504.

33 P. F. Smet, A. B. Parmentier, D. Poelman, *J. Electrochem. Soc*. **2011**, *158*, R37.

34 S. Allison, G. Gillies, A. Rondinone, M. Cates, *Nanotechnology* **2003**, *14*, 859.

35 E. Barberà, X. Tomàs, M. J. Moya, A. Ibàñez, M. B., Molins, J. Biosci. Bioeng. 1993, 76, 403.

36 V. D. Mihailetchi, H. X. Xie, B. d. Boer, L. J. A. Koster, P. W. M. Blom, *Adv. Funct. Mater*. **2006**, *16*, 699.

37 H. K. H. Lee, J. Wu, J. Barbé, S. M. Jain, S. Wood, E. M. Speller, Z. Li, F. A. Castro, J. R. Durrant, W. C. Tsoi, *J. Mater. Chem. A* **2018**, Advance Article

38 S. Yang, Z. Hsieh, M. L. Keshtov, G. D. Sharma, F. Chen, *Sol. RRL*. 2017, **1**, 1700174.

39 H. Yin, S. H. Cheung, J. H. L. Ngai, C. H. Y. Ho, K. L. Chiu, X. Hao, H. W. Li, Y. Cheng, S. W. Tsang, S. K. So, *Adv. Electron. Mater*. 2017, **3**, 1700007.

40 C. H. Y. Ho, Q. Dong, H. Yin, W. W. K. Leung, Q. Yang, H. K. H. Lee, S. W. Tsang,

S. K. So, *Adv. Mater. Interfaces*. 2015, **2**, 1500166.

41 D. L. Losee, *J. Appl. Phys*. 1975, **46**, 2204.

42 J. R. Yeargan, *J. Appl. Phys*. 1968, **39**, 5600.

43 H. Yin, P. Bi, S. H. Cheung, W. L. Cheung, K. L. Chiu, C. H. Y. Ho, H. W. Li, S. W. Tsang, X. Hao, S. K. So. *Sol. RRL*. 2018, **2***,* 17000239.

44 J. Costantini, G. Lelong, M. Guillaumet, W. J. Weber, S. Takaki, K. Yasuda, *J. Phys.: Condens. Matter*. 2016, **28**, 32.

45 C. H. Y. Ho, S. H. Cheung, H. Li, K. L. Chiu, Y. Cheng, H. Yin, M. H. Chan, F. So, S. W. Tsang, S. K. So, *Adv. Energy Mater*. 2017, **7**, 1602360.